

Soft Interface Fracture Transfer in Nanoscale MoS₂

Emily E. Hoffman¹  · Laurence D. Marks¹

Received: 7 June 2016 / Accepted: 17 August 2016
© Springer Science+Business Media New York 2016

Abstract Molybdenum disulfide (MoS₂) nanoflakes, nanotubes, and nanoparticles are used as solid lubricants and oil additives. We investigate the formation of transfer layers due to fracture during sliding on commercially available MoS₂ nanoflakes. The sliding and fracture properties were observed in high-frame-rate videos and high-resolution images captured using in situ transmission electron microscopy. The orientation of the flakes and the adhesion to the surface and to the contact asperity determined the weakest interface, which subsequently determined the fracture transfer layer. The fracture continued until both surface and counter surface lubricant layers were a single sheet. The fractured material created a transfer layer or wear particles. We did not observe the proposed “deck-of-cards” sliding, where the sliding is distributed between all the layers of a MoS₂ flake. Instead, we captured video of an entire flake fracturing at a weak point in the MoS₂ sheets, a “weakest link” soft interface fracture model. The soft interface fracture transfer (SIFT) model is not specific to MoS₂-layered nanoflakes, and we argue it is a general mechanism in the formation of tribolayers.

Keywords In situ · Transmission electron microscopy · Solid lubricants · Single asperity · Molybdenum disulfide

Electronic supplementary material The online version of this article (doi:10.1007/s11249-016-0743-2) contains supplementary material, which is available to authorized users.

✉ Laurence D. Marks
L-marks@northwestern.edu

¹ Department of Materials Science and Engineering,
Northwestern University, Evanston, IL 60208, USA

1 Introduction

Mitigating friction is a major challenge, especially with exposure to extreme thermal and environmental conditions. Many engineering systems rely on solid interfacial films to reduce friction and wear. Particularly, space-born systems depend on solid-phase lubrication, which include various movable devices such as gears, pumps, actuators, latches, antenna drives, and solar arrays [1, 2]. Transition metal dichalcogenides (MoS₂, WS₂, NbSe₂, etc.) are the most common solid lubricants for space and have growing applications as oil additives in regular machinery [3]. With these advanced applications, however, there are still many unknowns in the field of tribology, including the processes of lubrication and wear [4].

Surface asperity interactions of metal surfaces in contact were analyzed by Bowden and Tabor in the 1960s [5]; this work made it clear that many of the fundamental processes of tribology are taking place on the micron to nanoscale. For solid lubricants, analysis at the nanoscale and atomic scale allows for understanding of the fundamental properties of sliding. During asperity contact, sliding can cause material transfer from one surface to another. In the triboactive region, the region where sliding takes place, a number of phenomena can occur: solid lubricant transfer to contacting surface (transfer layers), third-body wear particles, rolling of particles, fracture, and recrystallization [6]. Wear products can keep evolving; such as wear particles attaching to one of the contacting surfaces to form a transfer layer.

At the macroscale, the friction of MoS₂ surface film depends on the integrity of the film, contact pressure, humidity, film thickness, temperature, and presence of contaminants [7, 8]. There are known wear modes of MoS₂, including deformation, fracture and reorientation,

fatigue-induced blistering, adhesive wear plowing, and abrasion by foreign particles [9, 10]. On the atomic scale, computation has shown that MoS₂ flakes can have friction anisotropy due to interlayer rotational misfit, showing that the orientation of the MoS₂ sheets determines the interactions of the sulfur atoms on the opposing sheets. This causes two orders of magnitude difference in friction [11]. It is crucial to bridge the atomic simulations to the micron-scale wear mechanism in MoS₂ in order to understand the formation of transfer layers [12].

On a microscopic scale, tribological wear processes studies have shown that tribolayers of softer materials can form through chip wear, where shearing off of the softer materials occurs at the asperity contact spot [12]. At the nanoscale, however, the formation and wear of transfer layers remain a topic of debate due to the buried interface problem: The triboactive layers and surfaces of interest are hidden and only accessible by post facto analysis, which leads to uncertainty.

At the nanoscale, MoS₂, along with the other dichalcogenide and the carbon solid lubricant graphite, has lubricating behavior stemming from an easy slip mode intrinsic to their crystal structure. MoS₂ is crystallized in a hexagonal structure, where a sheet of molybdenum atoms is sandwiched between two hexagonally packed sulfur layers. The bonding within the S–Mo–S sandwich is covalent, and weak Van der Waals forces hold the sandwich together resulting in easy interlamellar slip [6]. The shear of the sheets leads to transfer film formation on the rubbing counterface. Transfer layers of MoS₂ were recognized by Godet [13] and Singer [14], with studies by Wahl et al. [15] showing the formation of monolayers of crystalline MoS₂ following sliding and Hu et al. [16] investigating sheet alignment within ~500-nm-thick transfer layers. The complexity of lamellar lubricants is that lubrication depends on the fact that the reactivity of the basal plans is essentially zero so that they can slide with low friction; however, the basal plans also need to bond to the surfaces that are being lubricated [17, 18].

Understanding the mechanisms of tribolayer formation is critical to understanding wear and lubrication. In situ transmission electron microscopy imaging allows for recording of real-time behavior of triboactive layers and directly addresses the problem of viewing the buried interface. Over the last few years, there has been additional information available on nanoscale tribological processes made possible by in situ microscopy. For reviews of in situ developments, see work on general in situ [19], in situ TEM [20], and in situ single asperity [21]. In situ microscopy has shown that a single layer of MoS₂ can form a transfer layer and that the sheets slide against the counter MoS₂ surface [22]. Another study has shown interlayer shear stress of a single MoS₂ sheet attached to a charged

probe [23]. Mechanical properties of MoS₂ sheets, focusing on elastic bending and strain energy during cleaving, have highlighted the unique properties of MoS₂ [24–26]. For instance, Lahouij has shown crystalline nanoparticles of MoS₂ “exfoliating” single sheets or layers of sheets during in situ sliding tests [27–29]. The development of the tribolayer and creation of transfer layers, however, have not been clearly shown in situ for flakes of MoS₂.

Many have proposed the “deck-of-cards” model for sliding of lamellar lubricants, especially for MoS₂ [6, 22, 30, 31]. In this model, each S–Mo–S sheet is a “card,” which stacked up make the molecular layers of the crystal “deck.” When encountering lateral force on the top of the deck, each of the cards in the deck would slide, like pushing over a deck-of-cards. The nomenclature to describe the MoS₂ morphology and deck-of-cards is illustrated in Fig. 1. Each sheet takes on a fraction of the force; the sliding is distributed between each sheet of the MoS₂ flake. The deck-of-cards argument was also studied by Fleischauer et al. [17, 32–34]; it was framed in the context of intercrystalline slip versus intracrystalline slip. Deck-of-cards would be analogous to intercrystalline slip, with the lubrication coming from sliding between the basal planes distributed between all of the sheets. The counter idea is

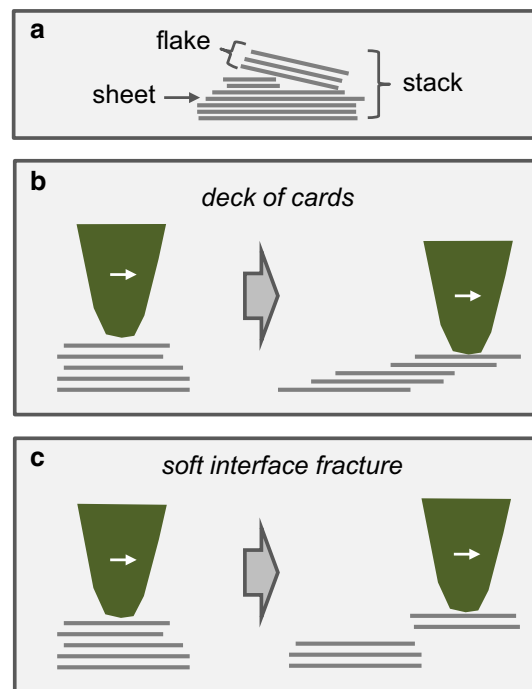


Fig. 1 **a** Diagram of the usual nomenclature used in the literature and in this paper. **b** Diagram of the commonly proposed “deck-of-cards” sliding, where each layer undergoes a fraction of the entire sliding. Here, the sliding is distributed throughout the entire flake. **c** Our results show the soft interface fracture sliding, where the sliding takes place in-between flakes or the in-between the most disordered sheets within a flake. The other parts of the stack remain stationary

intracrystalline slip, with the sliding between crystals, where the sliding is between lamella of adjoining crystallites. It was predicted that intracrystalline slip was likely because coatings of aligned, dense nanocrystalline MoS₂ had good friction and wear properties. Neither deck-of-cards nor intracrystalline slip phenomena, however, have been observed on the nanoscale. It is not yet clear how many (or how few) layers are needed to accommodate interfacial shear with low friction. Are one or more layers needed on both counter bodies? As Wahl and Sawyer [31] stated, “real-time TEM experiments hold the genuine possibility of answering the fundamental questions of how lamellar solid lubricants actually accommodate motion during sliding.”

In this study, in situ microscopy allows for nanoscale examination at the buried interface to see the fracture of stacks of nanoscale MoS₂ flakes. The fractured flake then forms a transfer layer. By imaging the interface and solid lubricant in real time through recording videos and high-resolution images, the behavior of nanoscale flakes was investigated in a variety of contact situations. The structures of MoS₂ flakes on the surface were observed before, during, and after contact with a single asperity. Through this setup, we observed that the contact force caused the MoS₂ flakes to fracture at the soft interfaces between partially aligned sheets. This fracture at the soft interfaces between MoS₂ flakes during sliding created transfer layers, which we describe here in terms of a soft interface fracture transfer (SIFT) model. The fracture here is not intercrystalline slip, but occurs between the nanoflakes as intracrystalline slip. We propose that the SIFT layers and mechanism are general in the creation and behavior of transfer layers in lamellar solid lubricant systems.

2 Experimental

The sample was made from a fragment of a Si aperture TEM grid, fractured into about four pieces. The Si fractured along crystallographic planes to create a thin, electron-transparent edge. The MoS₂ nanoflakes are commercially available from Graphene Supermarket as Molybdenum Disulfide Pristine Flakes. The nanoflakes came in a dispersed solution, and the company indicated size of the nanoflakes was accurate. For sample preparation, approximately 10–15 drops were deposited on the Si fragment. The fragment sat on a hotplate set to 55 °C to speed solution evaporation. The sample was glued on a tungsten needle with M-bond to fit in the TEM sample holder mount.

An FEI Tecnai F20ST TEM at Argonne National Laboratory operated at 200 kV was employed for the in situ sliding tests. The sliding occurred in the vacuum

environment of the TEM at less than 1×10^{-7} Torr. The experimental setup of the Nanofactory TEM/AFM holder is shown in Fig. 2. A silicon AFM tip fabricated on a cantilever was used as the sliding counterpart with a spring constant of 5.6 N/m as provided by the vendor [35]. The sample can move three-dimensionally in the holder in the TEM. The sample movement is driven by a piezomotor with resolutions of 0.2 Å in XY and 0.025 Å in Z. The sliding experiments took place at no load (within measurement error) with no detectable cantilever deflection.

The processes were recorded using a TV-rate video camera. The extracted frames were processed by deinterlacing and adjusting the levels for clarity using the program GIMP. Videos of the in situ sliding tests are available in the Online Resources.

3 Results

Three areas of ideal MoS₂ flakes were found in the TEM, with the MoS₂ sheets oriented parallel to the beam direction. Most flakes were between 30 and 150 nm long and 5–20 sheets thick. Sheet depth was assumed to be on the order of the flake length. The well-oriented stacks of flakes consisted of 2–3 clearly defined flakes. Figure 3 shows the three examples of stacks of MoS₂ flakes that occurred on the edge of the Si substrate. The initial state is shown in Fig. 3a-1, b-1, and c-1; here the stacks were in their original arrangement, untouched by the AFM tip. Examples a-1 and c-1 had two flakes in the stack, and example b-1 had three flakes in the stack.

Within a stack of flakes, the distinction between flakes was identifiable by the disorder between the sheets of MoS₂. Within a single flake, the sheets are of approximately the same length and have few to no defects along the interface of the sheets. In the TEM, the order is observable by the straight and clear sheets that appear as black lines. In contrast, between flakes there is a misorientation with layers of half sheets (dislocations) inserted between the flakes. These disordered interface layers disrupt structure and Van der Waals bonding of the sheets.

To begin the sliding experiments, the AFM tip, representing a single asperity, was brought into contact with the stack of flakes, making contact at the top of the top flake, as seen in the three examples in Fig. 3. When the AFM came within ~ 4 nm of the top flake, the AFM tip would jump to adhesion. The sample was moved into the AFM tip to a compressive force and then brought back down to slide at neutral force; there was no AFM cantilever deflection during sliding. This adhesion and the sliding motion thereafter caused fracture within the stack of flakes. The fracture occurred at the weakest interface, which was the interface between the flakes that had the most disorder. The

Fig. 2 Experimental setup of the in situ sliding test. **a** Photograph of the holder with mounted sample. **b** Drawing to show the orientation of the fractured Si edge and AFM tip orientation. **c** TEM image of the boxed region showing the sample, AFM tip, and an arrow to a MoS₂ flake on the edge

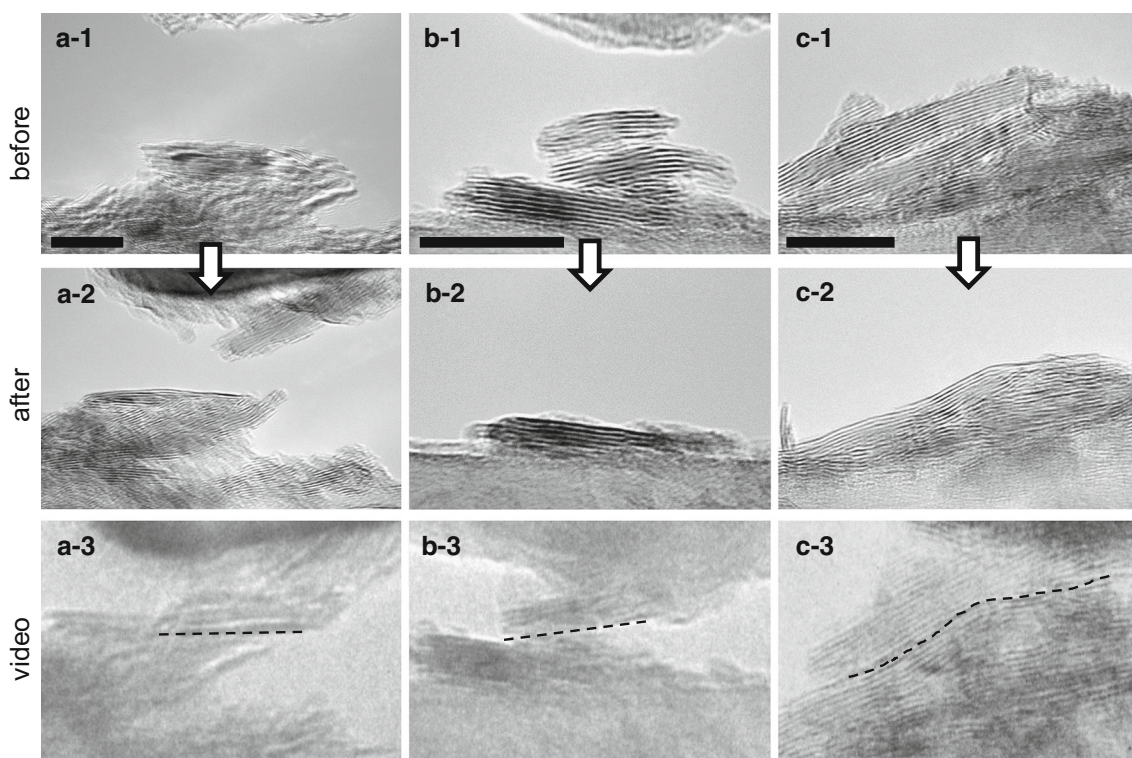
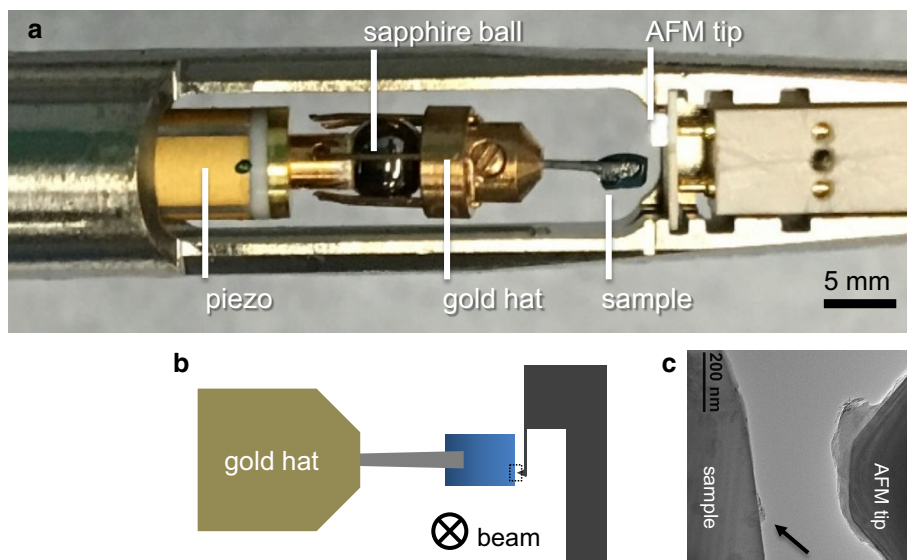


Fig. 3 Three examples of soft interface fracture transfer layers forming, with initial states of (a-1), (b-1), and (c-1) and final states after fracture of the transfer layer of (a-2), (b-2), and (c-2). (a-3), (b-

3), and (c-3) show extracted video frames with the dotted line showing the soft interface. Scale bars are 20 nm

videos of Fig. 3a–c are in Online Resources 1–3, respectively.

For examples a and c in Fig. 3, the weakest interface was the boundary between the top flake and bottom flake, with stronger adhesion of the top flake to the AFM tip and the bottom flake to the Si substrate. For example b with three flakes, the weakest interface was between the middle and bottom flake. This is due to the

orientation of the flakes. As seen in Fig. 3b-1, the top and middle flakes are parallel, whereas there is a misorientation of 18° between the middle and bottom flakes. The transfer layers can be seen mid-slide in Figs. 3a-3 and 2b-3, c-3, which were extracted from the videos from Online Resources 1, 2, and 3, respectively. The flake that fractures and transfers to the tip created the transfer layer.

As MoS₂ can wear in various modes, we also observed SIFT layers occurring with rolling MoS₂ flakes. During experimental sliding, a flake of MoS₂ 25 nm in diameter was rolled between the AFM tip and the Si surface, as shown in Fig. 4a, b from extracted frames from Online Resource 4. For this SIFT example in particular, the rolling was better captured in the video of Online Resource 4 than in the extracted frames of Fig. 4. When rolling, the ball encountered oriented stacks of MoS₂ flakes and changed from rolling to sliding; sliding became the mode of least

friction. The sliding is seen in Fig. 4c–f, again extracted from Online Resource 4. The top transfer flake of ~three layers, in Fig. 4f, fractured from the bottom flakes on the Si surface and transferred to the ball. The fracture interface was the weakest interface in the flake. Figure 5a shows an image of the area before sliding. Then, the extracted video frame in Fig. 5b shows the transfer sheets moving to the ball and the bottom sheets adhering to the Si surface.

The sliding system is a dynamic process. The adhesion to the contacting interface, the tip in this case, was not

Fig. 4 **a** Ball of MoS₂ rolled between the AFM tip and the Si surface. **b** The feature rolled without slipping, indicated by the *circle markers*. **c** The ball hit the oriented MoS₂ flakes and changed from rolling to sliding. **d, e** The sliding of the transfer flake. **f** The top flake as a transfer flake on the ball. **c–f** include an orientation marker to show the ball stopped rolling and the *black arrow* points to the transfer flake. *Scale bar* is 20 nm

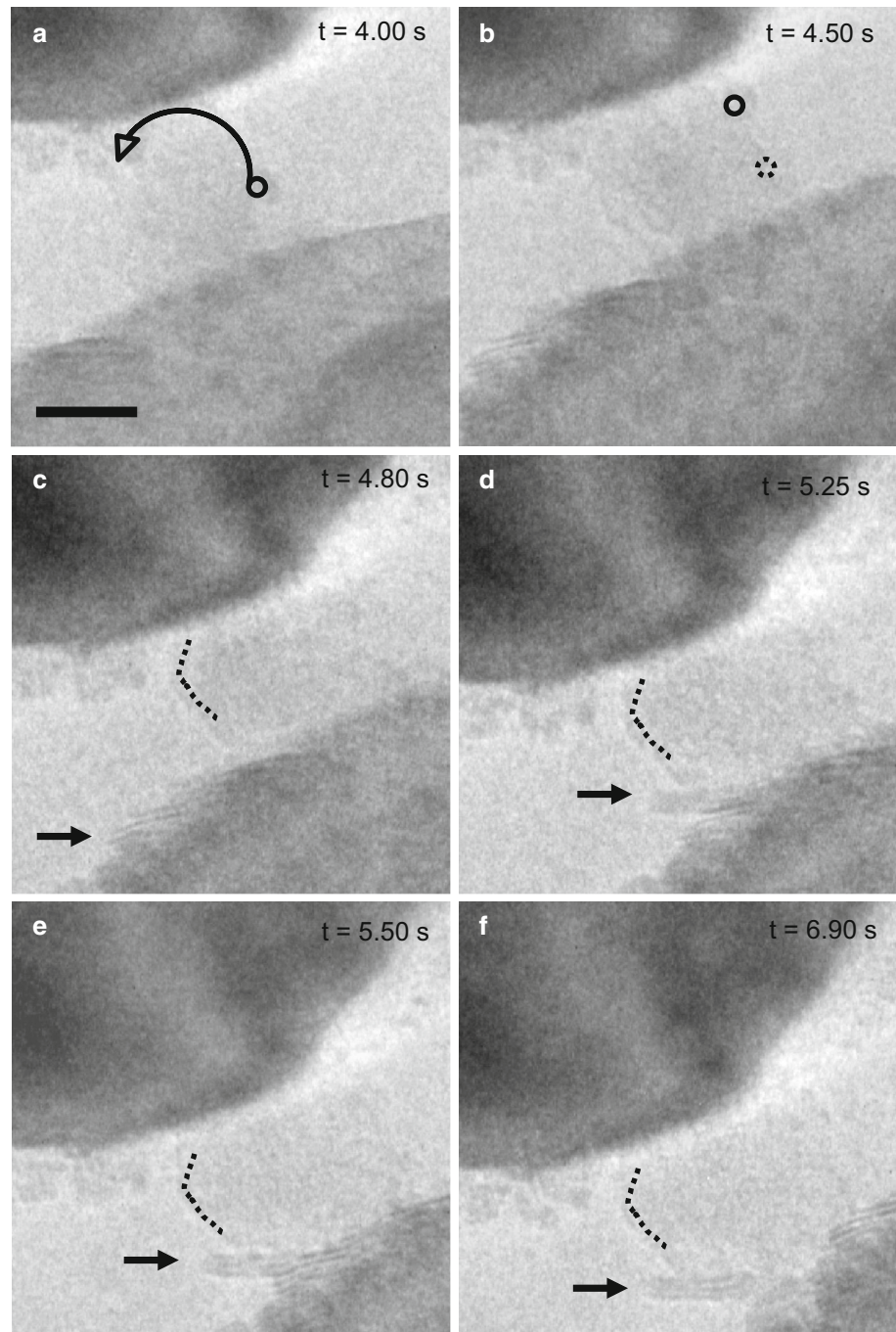
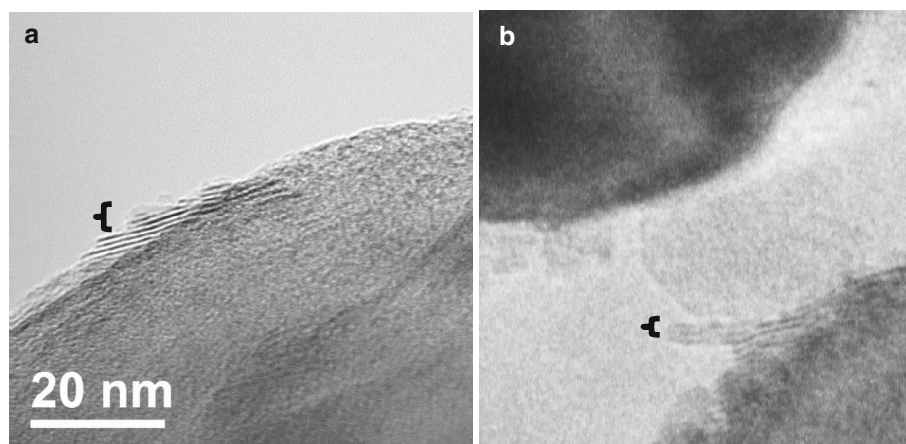


Fig. 5 **a** Area before any contact with the future transfer flake noted with the *bracket* and **b** the same sheets adhered to the sliding ball. *Scale bar* is 20 nm



permanent. Other attractive forces caused the transfer flake to jump back to the Si surface, usually at a random location and orientation. The transfer flake from Fig. 3 example c is again highlighted in Fig. 6. The stages of sliding are depicted in Fig. 6a–c (extracted from Online Resource 3), and the jump of the transferred layer back to the substrate is seen in Fig. 6d (extracted from Online Resource 5). After fracturing from the bottom flake, transferring to the AFM tip, and jumping back to the substrate surface, it is notable that the sheets left intact on the flake were highly aligned. These were the most strongly bonded to the substrate, where the other partial sheets of the flake fractured off to other more attractive surfaces during the transition jumps.

The fracture transfer layers occurred because there was a soft interface between the sheets, the weakest point in the stack of flakes. The soft interface is clearly seen in Fig. 7

when the top transfer flake from Fig. 3 example b was brought back in contact with the bottom flake and then slid back and forth. Figure 7a–c shows the Si substrate sliding right and the transfer flake conforming in shape to have maximum alignment with both the AFM tip above and the sheet of MoS₂ on the bottom flake beneath. Then in Fig. 7d–f, as the substrate is slid to the left, the flake continues to attract to both surfaces and forms evolving soft interfaces. Video of the process depicted in Fig. 7 is found in the second half of Online Resource 2. The SIFT layer curled and bent to keep the most contact with the soft interface, as this contact is the lowest energy orientation.

To show the evolution of soft interface fracture, sliding was continued until no more fracture occurred within a stack of flakes. The stack of flakes in Fig. 3 example b was used to continue sliding, with the extracted frames from the video in Fig. 8. First, the initial fracture event occurred,

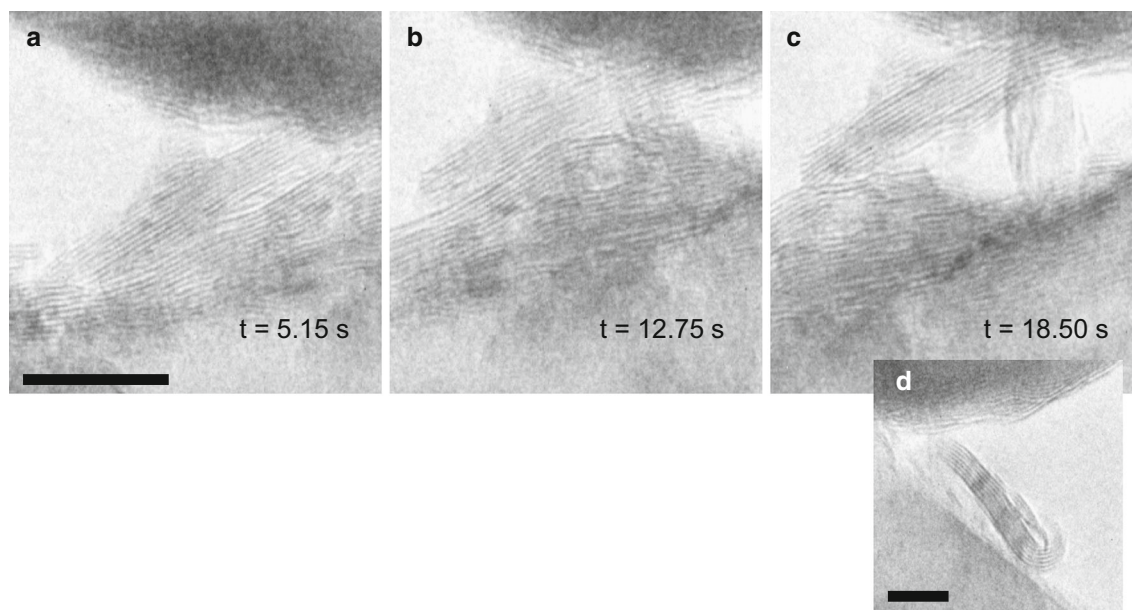


Fig. 6 **a–c** Stages of the SIFT layer sliding from the bottom flake, and **d** adhesion to the Si surface after SIFT. *Scale bar* is 20 nm

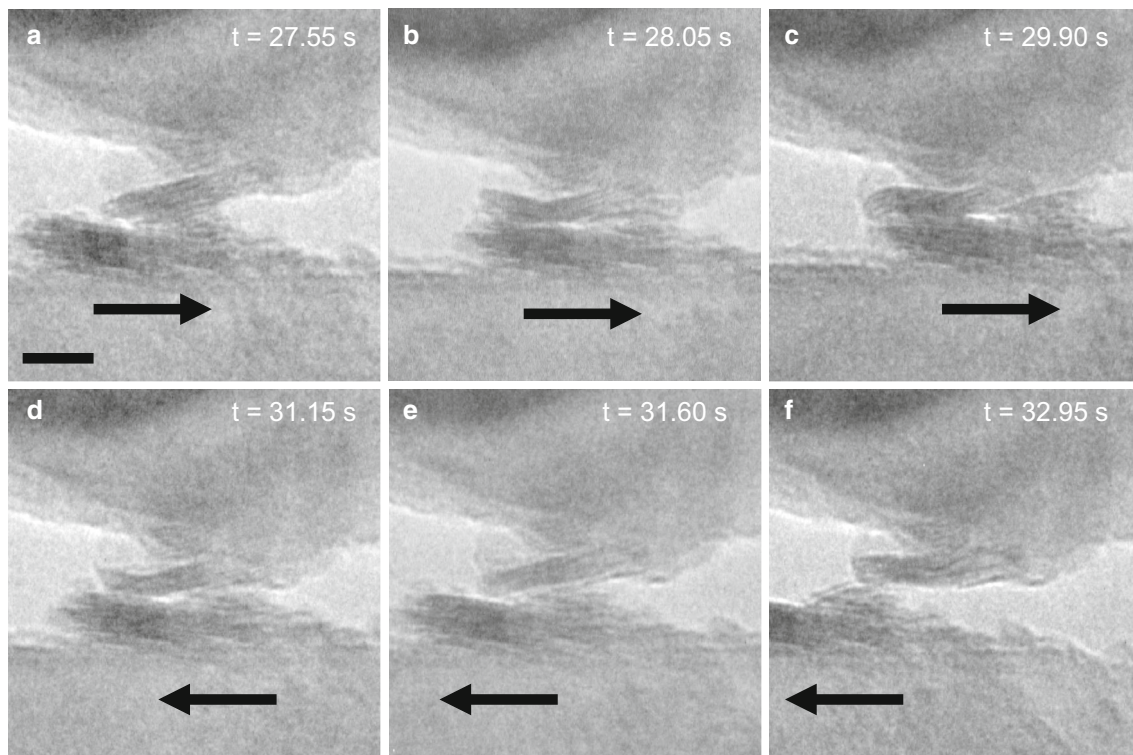


Fig. 7 a–c Si substrate *slid right* and d–f *slid left* to highlight the bending of the transfer flake, showing the evolving soft interface. Scale bar is 10 nm

shown in Fig. 3, where the top two flakes became a transfer layer, Fig. 8a, b. Next, the transfer layer was slid gently back and forth on the bottom stack, shown in Fig. 8b, c. (The detail of the sliding step is in Fig. 6). In Fig. 8c, the transfer flake became adhered to the tip shape and some sheets were worn away. These minor instances of soft interface fracture from Fig. 8c, d are seen in Online Resource 6. The initial stack was made of three clear flakes, but in Fig. 8c–e, a smaller partial flake stayed adhered to the bottom flake. The partial flake’s misalignment to the bottom flake was only 10° . A coarse slide occurred between Fig. 8d, e, which caused the partial flake to fracture at the soft interface. This fracture is seen in Online Resource 7. From this series of fractures, the four weakest soft interfaces are apparent. The final state of the stack, Fig. 8e, resulted in a flake parallel to the substrate. The tip tribolayer became conformal to the tip shape. Both the tribolayers and the flake surfaces ended with primarily continuous sheets at the sliding interface. At this state, dozens of sliding passes occurred with no change in morphology. Here, no soft interfaces were present and sliding had become stable. The end state soft interface fracture is explained in depth for Fig. 3 example 2, and it was also observed for example 1 and 3.

4 Discussion

Here, we observed the buried interface of MoS_2 nanoflakes between a Si surface and a Si AFM tip using in situ electron microscopy. Through contact with the AFM tip asperity, the stacks of MoS_2 flakes fractured at soft interfaces between disordered sheets. The soft fracture of an entire flake created a soft interface fracture transfer layer. The “deck-of-cards” model, where sliding is distributed between every sheet of a MoS_2 flake, was not observed. The SIFT layer explains how transfer layers form during lamellar solid lubrication.

The SIFT layer formation is, most simply, a weakest link mechanism. The slip we saw was not intercrystalline, not collective between the lamella, but it was intracrystalline slip, between individual nanoflakes. Instead of the deck-of-cards model, a more appropriate description would be links in a chain. When stressed, the weakest link breaks. If one of the pieces of the broken chain is again stressed, there is a new weakest link where fracture will occur. The weakest link as the source of failure is inherent throughout materials and size scales. It is rare that a macroscale intuition can apply down to the nanoscale, but here the “weakest link” model aptly describes the behavior.

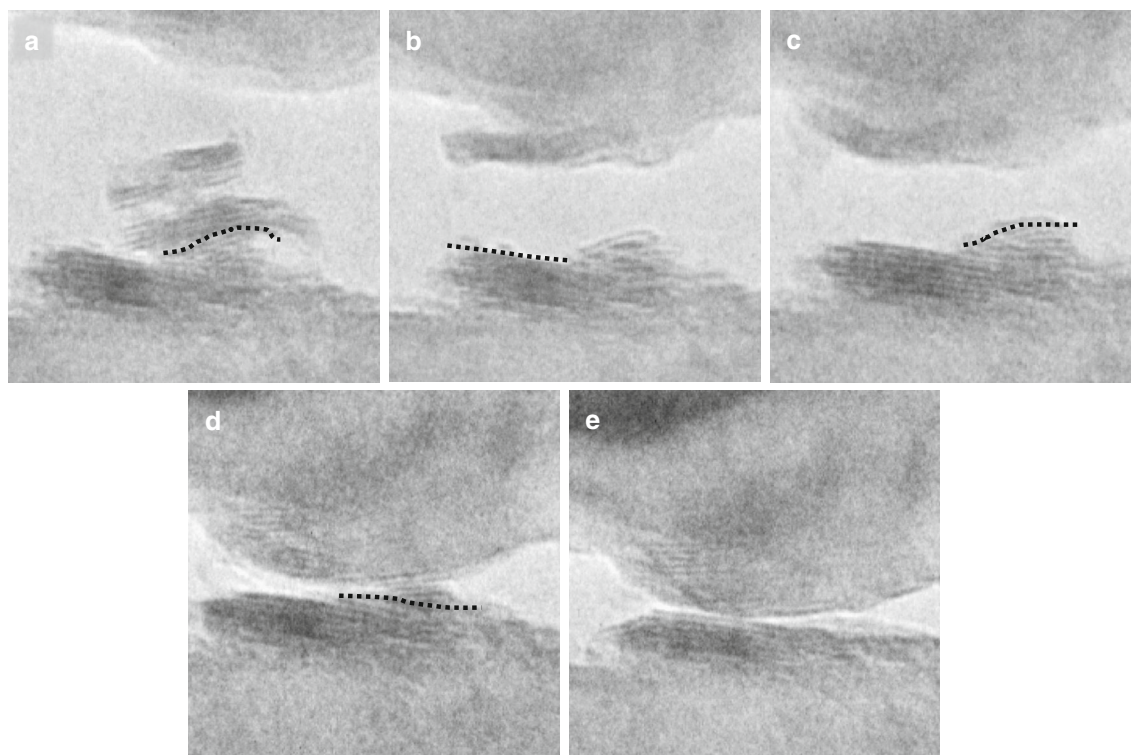


Fig. 8 Soft interface fracture process of the stack of flakes from Fig. 2 example b. **a** The initial stack fractures at the weakest interface indicated with the *dotted line*. **b** The SIFT layer is created on the tip, and the next soft interface fracture point is indicated with the *dotted line*. **c** The transfer layer has adhered to the shape of the tip, and

further removal of the weakest layers is seen. **d** The last misaligned flake is indicated with the *dotted line*. **e** All misaligned flakes are removed from both the initial stack and from the transfer layer as well. Both the flake on the substrate's and the transfer flake's surfaces are made of a primarily continuous sheet of MoS₂

An alternative, more mathematical way of making the same statement is to consider the activation energy barrier to deformation. Slip has to involve dislocations, either localized or delocalized depending upon the local bonding. In a pristine material for slip to start dislocation, loops (or half loops) have to nucleate, a substantial energy barrier. When defects already exist, the activation energy to nucleate defects is no longer required. Hence, slip occurs at where dislocations already exist, for instance at interfaces (assuming that the relevant slip systems are available). For the deck-of-cards mechanism, it would have to be energetically favorable to simultaneously create a number of dislocations and have them moved in a concerted fashion. While this is not impossible and could occur at existing low angle boundaries, it is unlikely at the small sizes herein.

In MoS₂ and in other lamellar lubricants, the weakest link is the layer with the most disorder. The forces presented in these stacks are covalent bonds and Van der Waals bonds. The sheets of MoS₂ are covalently bonded, and these are not changing. The Van der Waals bonding occurs between the sheets of the MoS₂ flakes, and they also occur between the flakes and the Si substrate and Si tip (referred to as adhesion). Within stacks of flakes, disorder is most obviously seen in misorientation between flakes. In

the three-flake stack example presented, in Fig. 8, the initial fracture is between the flakes with the largest misalignment (the middle and bottom flake, 18°, Fig. 8a, b). Next, there are sheets and small flakes removed from the top of the substrate flake and from the bottom of the transfer layer flake (Fig. 8b–d). Lastly, it takes a coarse, larger force to fracture the less aligned flakes (the partial flake and bottom flake, 10°, Fig. 8d, e). Through this evolution of flake morphology, we can see the hierarchy of weakest links. We see the major SIFT layers that create the initial transfer layer, but then we can also see minor soft interface fracture of partial layers. The surface refinement process is seen in Fig. 8 as the partials imperfect flakes are removed.

The SIFT mechanism is a generic process. It can be subdivided by the type of fracture process that occurs: Mode I (fracture in tension caused by adhesion), versus Mode II or III (caused by shear) [36]. In our system in vacuum with freshly cleaved Si surfaces, the adhesion is strong between the MoS₂ nanoflakes and the Si. This allows our study to primarily focus on Modes II and III, shearing creation of the transfer layers. If we were to pull straight back to focus on Mode I, the soft interface fracture would not occur the same way—but would still occur.

We observe an endgame of the weakest link model once the most significant soft interfaces have been fractured. After the major SIFT layer fracture occurs, it can be inferred that the partial flake on the bottom flake, pictured in Fig. 8d, had stronger Van de Waals bonding than the transfer layer flake. The stronger bonding was due to the higher order between the sheets. There are not enough defects in the bonding between any of the partial flake layers for fracture to occur with the same level of force. This was a metastable state. Therefore, a larger force than the standard piezomotor was needed to fracture the partial flake, Fig. 8d, e. At this point in sliding, Fig. 8e, no soft interfaces were apparent, and sliding had reached a stable state. Both the Van de Waals bonding within the crystalline nanoflake and the adhesion between the flake and the Si were higher than the Mode I fracture force. The Mode I fracture stress came from bringing the counterface flake in contact and pulling apart. We are further evaluating the various fracture modes and when the nanoflakes stop wearing from adhesion and sliding forces in future work.

The intracrystalline slip observation supports the idea that best performing MoS₂ films should be made with small crystallites, such as the nanoflakes used here, because dense crystallites enable stable sliding lamellae surfaces to be generated on each face with only a small amount of the film wearing away in the process. At least one soft interface within the material is needed to create a transfer layer, but if you have all soft interfaces, the crystallites (nanoflakes in our experiments) will continuously break down until the film is gone. The in situ observations here have helped to establish the connection of how crystallites are free to move and be transferred, previously discussed by Fleischauer [17, 18].

Further methods to understand the weakest link SIFT model would require measuring the force, approach angle, flake orientations, and adhesion. These factors contribute to soft interface fracture and the creation of a stable sliding interface. Metastable states were observed at some constant force sliding or for a limited number of passes. The final stable point was two complete sheets of MoS₂, one on the substrate and one on the asperity, as the sliding interface. In that case, soft interfaces were no longer present, except for the sliding interface.

These MoS₂ sliding experiments highlight that tribology is the study of weak interfaces. The creation, wear, and fracture at these soft interfaces need to be well understood to be able to control the lubrication process. The soft interfaces allow for transfer layers to occur in lamellar solid lubricants and also explain how the triboactive surfaces wear into a stable state.

Acknowledgments This work was funded by the NSF under the Grant Number CMMI-1030703. EEH is funded through the National

Defense Science and Engineering Graduate Fellowship. Portions of this work were performed in the Electron Microscopy Center of the Center for Nanoscale Materials at Argonne National Laboratory, a US Department of Energy, Office of Science, Office of Basic Energy Sciences User Facility under Contract No. DE-AC02-06CH11357.

References

- Conley, P.L.: *Space Vehicle Mechanisms: Elements of Successful Design*. Wiley, New York (1998)
- Voevodin, A., Zabinski, J.: Nanocomposite and nanostructured tribological materials for space applications. *Compos. Sci. Technol.* **65**(5), 741–748 (2005). doi:[10.1016/j.compscitech.2004.10.008](https://doi.org/10.1016/j.compscitech.2004.10.008)
- Rabaso, P., Ville, F., Dassenoy, F., Diaby, M., Afanasiev, P., Cavoret, J., Vacher, B., Le Mogne, T.: Boundary lubrication: influence of the size and structure of inorganic fullerene-like MoS₂ nanoparticles on friction and wear reduction. *Wear* **320**, 161–178 (2014). doi:[10.1016/j.wear.2014.09.001](https://doi.org/10.1016/j.wear.2014.09.001)
- Singer, I.L.: Mechanics and chemistry of solids in sliding contact. *Langmuir* **12**(19), 4486–4491 (1996). doi:[10.1021/la951056n](https://doi.org/10.1021/la951056n)
- Bowden, F., Tabor, D.: *Friction and Lubrication of Solids*, vol. I. Clarendon, Oxford (1950)
- Scharf, T.W., Prasad, S.V.: Solid lubricants: a review. *J. Mater. Sci.* **48**(2), 511–531 (2013). doi:[10.1007/s10853-012-7038-2](https://doi.org/10.1007/s10853-012-7038-2)
- Holmberg, K., Matthews, A.: *Coatings Tribology: Properties, Mechanisms, Techniques and Applications in Surface Engineering*. Elsevier, Amsterdam (2009)
- Sliney, H.E.: Solid lubricant materials for high temperatures—a review. *Tribol. Int.* **15**(5), 303–315 (1982). doi:[10.1016/0301-679x\(82\)90089-5](https://doi.org/10.1016/0301-679x(82)90089-5)
- Singer, I.L., Pollock, H.: *Fundamentals of Friction: Macroscopic and Microscopic Processes*, vol. 220. Springer, Braunlage (2012)
- Singer, I.L., Dvorak, S.D., Wahl, K.J., Scharf, T.W.: Role of third bodies in friction and wear of protective coatings. *J. Vac. Sci. Technol., A* **21**(5), S232–S240 (2003). doi:[10.1116/1.1599869](https://doi.org/10.1116/1.1599869)
- Onodera, T., Morita, Y., Nagumo, R., Miura, R., Suzuki, A., Tsuboi, H., Hatakeyama, N., Endou, A., Takaba, H., Dassenoy, F., Minfray, C., Joly-Pottuz, L., Kubo, M., Martin, J.M., Miyamoto, A.: A computational chemistry study on friction of h-MoS(2). Part II. Friction anisotropy. *J. Phys. Chem. B* **114**(48), 15832–15838 (2010). doi:[10.1021/jp1064775](https://doi.org/10.1021/jp1064775)
- Ribarsky, M.W., Landman, U.: Microscopic mechanisms of tribological and wear processes: molecular dynamics simulations. In: *Approaches to Modeling of Friction and Wear: Proceedings of the Workshop on the Use of Surface Deformation Models to Predict Tribology Behavior*, Columbia University in the City of New York, 17–19 December 1986. pp. 159–166. Springer, New York (1988)
- Godet, M.: The third-body approach: a mechanical view of wear. *Wear* **100**(1–3), 437–452 (1984). doi:[10.1016/0043-1648\(84\)90025-5](https://doi.org/10.1016/0043-1648(84)90025-5)
- Singer, I.L., Fayeulle, S., Ehni, P.D.: Friction and wear behavior of tin in air—the chemistry of transfer films and debris formation. *Wear* **149**(1–2), 375–394 (1991). doi:[10.1016/0043-1648\(91\)90386-9](https://doi.org/10.1016/0043-1648(91)90386-9)
- Wahl, K.J., Dunn, D.N., Singer, I.L.: Wear behavior of Pb–Mo–S solid lubricating coatings. *Wear* **230**(2), 175–183 (1999). doi:[10.1016/s0043-1648\(99\)00100-3](https://doi.org/10.1016/s0043-1648(99)00100-3)
- Hu, J.J., Wheeler, R., Zabinski, J.S., Shade, P.A., Shiveley, A., Voevodin, A.A.: Transmission electron microscopy analysis of Mo–W–S–Se film sliding contact obtained by using focused ion beam microscope and in situ microtribometer. *Tribol. Lett.* **32**(1), 49–57 (2008). doi:[10.1007/s11249-008-9360-z](https://doi.org/10.1007/s11249-008-9360-z)

17. Fleischauer, P.D., Bauer, R.: The influence of surface chemistry on MoS₂ transfer film formation. *ASLE Trans.* **30**(2), 160–166 (1987)
18. Miyoshi, K., Chung, Y.: *Surface Diagnostics in Tribology: Fundamental Principles and Applications*. World Scientific, Singapore (1993)
19. Sawyer, W.G., Wahl, K.J.: Accessing inaccessible interfaces: in situ approaches to materials tribology. *MRS Bull.* **33**(12), 1145–1150 (2008)
20. Marks, L.D., Warren, O.L., Minor, A.M., Merkle, A.P.: Tribology in full view. *MRS Bull.* **33**(12), 1168–1173 (2008). doi:[10.1557/mrs2008.247](https://doi.org/10.1557/mrs2008.247)
21. Liao, Y., Marks, L.: In situ single asperity wear at the nanometre scale. *Int. Mater. Rev.* (In production) (2016)
22. Casillas, G., Liao, Y., Jose-Yacamán, M., Marks, L.D.: Monolayer transfer layers during sliding at the atomic scale. *Tribol. Lett.* **59**(3), 1–5 (2015). doi:[10.1007/s11249-015-0563-9](https://doi.org/10.1007/s11249-015-0563-9)
23. Oviedo, J.P., Kc, S., Lu, N., Wang, J., Cho, K., Wallace, R.M., Kim, M.J.: In situ TEM characterization of shear–stress-induced interlayer sliding in the cross section view of molybdenum disulfide. *ACS Nano* **9**(2), 1543–1551 (2015). doi:[10.1021/nm506052d](https://doi.org/10.1021/nm506052d)
24. Castellanos-Gomez, A., Poot, M., Steele, G.A., van der Zant, H.S., Agrait, N., Rubio-Bollinger, G.: Elastic properties of freely suspended MoS₂ nanosheets. *Adv. Mater.* **24**(6), 772–775 (2012). doi:[10.1002/adma.201103965](https://doi.org/10.1002/adma.201103965)
25. Casillas, G., Santiago, U., Barrón, H.C., Alducin, D., Ponce, A., José-Yacamán, M.: Elasticity of MoS₂ Sheets by mechanical deformation observed by in situ electron microscopy. *J. Phys. Chem. C* **119**(1), 710–715 (2014)
26. Tang, D.M., Kvashnin, D.G., Najmaei, S., Bando, Y., Kimoto, K., Koskinen, P., Ajayan, P.M., Yakobson, B.I., Sorokin, P.B., Lou, J., Golberg, D.: Nanomechanical cleavage of molybdenum disulfide atomic layers. *Nat Commun.* **5**, 3631 (2014). doi:[10.1038/ncomms4631](https://doi.org/10.1038/ncomms4631)
27. Lahouij, I., Dassenoy, F., de Knoop, L., Martin, J.M., Vacher, B.: In situ TEM observation of the behavior of an individual full-erene-like MoS₂ nanoparticle in a dynamic contact. *Tribol. Lett.* **42**(2), 133–140 (2011). doi:[10.1007/s11249-011-9755-0](https://doi.org/10.1007/s11249-011-9755-0)
28. Lahouij, I., Vacher, B., Dassenoy, F.: Direct observation by in situ transmission electron microscopy of the behaviour of IF-MoS₂ nanoparticles during sliding tests: influence of the crystal structure. *Lubr. Sci.* **26**(3), 163–173 (2014)
29. Tannous, J., Dassenoy, F., Lahouij, I., Le Mogne, T., Vacher, B., Bruhacs, A., Tremel, W.: Understanding the tribochemical mechanisms of IF-MoS₂ nanoparticles under boundary lubrication. *Tribol. Lett.* **41**(1), 55–64 (2011). doi:[10.1007/s11249-010-9678-1](https://doi.org/10.1007/s11249-010-9678-1)
30. Singer, I.L.: How third-body processes affect friction and wear. *MRS Bull.* **23**(6), 37–40 (1998). doi:[10.1557/S088376940003061X](https://doi.org/10.1557/S088376940003061X)
31. Wahl, K.J., Sawyer, W.G.: Observing interfacial sliding processes in solid–solid contacts. *MRS Bull.* **33**(12), 1159–1167 (2011). doi:[10.1557/mrs2008.246](https://doi.org/10.1557/mrs2008.246)
32. Hilton, M.R., Fleischauer, P.D.: Structural studies of sputter-deposited MoS₂ solid lubricant films. In: *MRS Proceedings 1988*, p. 227. Cambridge University Press, Cambridge
33. Hilton, M.R., Fleischauer, P.D.: TEM lattice imaging of the nanostructure of early-growth sputter-deposited MoS₂ solid lubricant films. *J. Mater. Res.* **5**(02), 406–421 (1990)
34. Fleischauer, P.D., Bauer, R.: Chemical and structural effects on the lubrication properties of sputtered MoS₂ films. *Tribol. Trans.* **31**(2), 239–250 (1988)
35. Nafari, A., Karlen, D., Rusu, C., Svensson, K., Olin, H., Enoksson, P.: MEMS sensor for in situ TEM atomic force microscopy. *J. Microelectromech. Syst.* **17**(2), 328–333 (2008). doi:[10.1109/jmems.2007.912714](https://doi.org/10.1109/jmems.2007.912714)
36. Bhushan, B.: *Modern Tribology Handbook, Two Volume Set*. CRC Press (2000)